The Ultra High Resolution QuikSCAT Product

Brent A. Williams, Michael P. Owen, and David G. Long
Brigham Young University, 459 CB, Provo, UT 84602

***Abstract*— Although QuikSCAT was originally designed to measure winds at a resolution of 25km, higher resolution wind and rain products have been developed. The 2.5km ultra high resolution (UHR) products allow QuikSCAT data to be used for applications involving rain, meso-scale phenomena, and in coastal applications. This paper overviews and unifies the various UHR products and discusses their advantages and limitations as compared to each other and the conventional 25km product. Theory, consequences of assumptions, and trade-offs are also discussed.**

I. Introduction

The normalized radar cross section (σ^0) of the ocean surface varies with the near-surface wind field and with the rain rate. This relationship between the vector wind, the rain rate, and σ^0 is described by an empirically derived geophysical model function (GMF). Using the GMF, it is possible to estimate the wind and rain over the ocean from σ^0 measurements from different azimuth angles.

The QuikSCAT scatterometer is a spaceborne radar originally designed to measure wind over the ocean at a resolution of 25km (25km spacing between point-wise wind estimates). This resolution is suitable for global scale wind structures. However, the resolution of this product is a limiting factor for applications involving rain, storm and meso-scale structures, or in coastal regions. Even large storms such as hurricanes may not be well resolved by the standard 25km product (the Jet Propulsion Laboratory's level 2B (L2B) product). Furthermore, rain is generally a smaller scale feature than wind. Coastal studies with the 25km product are limited to regions at least 30km from land because the high σ^0 value from land contaminates the relatively low value over the ocean causing the wind estimates in regions close to land to be unreliable.

Over the past few years several ultra high resolution (UHR) wind and wind/rain products have been developed which ameliorate some of the resolution-related issues of QuikSCAT data [1] [2] [3] [4] [5]. Each of these UHR products employ incoherent reconstruction of the spatial σ^0 field (image) to obtain a high spatial resolution (pixel spacing) of 2.5km for the σ^0 field. Point-wise wind-only or simultaneous wind/rain estimation are then performed on each 2.5km pixel. While the UHR wind/rain estimates are noisier than conventional products, with care they can enable the use of QuikSCAT data to study smaller scale wind and rain structures as well as provide estimates closer to land.

This paper overviews and unifies the various UHR products, while discussing their advantages and limitations as compared to each other and to the conventional 25km product. The theory (including the derivation of the noise and measurement model) is presented, assumptions and approximations are explored, and trade-offs are discussed. A description of the unified UHR product is also provided.

II. Measurement models

This section presents and compares the measurement models used in conventional and UHR QuikSCAT processing. Relevant properties of the QuikSCAT sensor are also stated.

QuikSCAT is a Ku-band scatterometer with two conical scanning beams (one vertical polarization at a nominal incidence angle of 54^o, and one horizontal polarization at a nominal incidence angle of 46^o) [6]. This provides four "flavors" (v- and h-pol, fore- and aft-looking) of σ^0 over most of the QuikSCAT swath with only two flavors in the outer swath (v-pol fore- and aft-looking). QuikSCAT is a pulsed radar system with a square-law detection measurement scheme. The backscattered power from the Earth's surface for each pulse is partitioned into several slices using range-Doppler processing. The measured power is scaled by the parameters in the radar equation (spreading losses, system losses, gain, and effective slice spatial response functions) to produce a separate normalized radar cross section (σ^0) measurement for each slice. The noisy slice measurements are modeled as Gaussian random variables with the mean as the true σ^0 value, and a variance that is a function of the mean (due to Rayleigh fading). The standard model of the noisy slice measurement for slice s_i can be written as $\sigma^0_{m,s_i} = \sigma^0_{t,s_i}(1 + K_{p,s_i}\nu_{s_i})$ where ν_{s_i} is a zero mean unit variance Gaussian random variable, σ^0_{t,s_i} is the 'true' slice σ^0 value, and $K_{p,s_i} = \sqrt{var\{\sigma^0_{m,s_i}\}}/\sigma^0_{t,s_i}$ is the normalized standard deviation. Note that $\sigma^0_{t,s_i} = E\{\sigma^0_{m,s_i}\}$, and that K_{p,s_i} is a function of the scatterometer design and embodies the variability due to system noise as well as Rayleigh fading. When performing wind/rain retrieval, K_{p,s_i} may be augmented to also describe the uncertainty in the GMF.

For the conventional 25km processing the slices in each pulse of a given beam are averaged together into 'egg' measurements. The standard QuikSCAT GMF relates the mean of the noisy egg measurements to the wind vector where the azimuth and incidence angles are the azimuth and incidence angle of the egg center. The conventional wind retrieval method assumes that the wind field is constant over each 25km×25km wind vector cell. Each egg measurement whose center falls into a wind vector cell is used to estimate the wind speed and direction of that wind vector cell [6]. Rain can degrade the wind estimate accuracy [7] and so cells con-

978-1-4244-2871-7/09/$25.00 ©2009 IEEE

taining significant rain rates are flagged. Averaging the slice measurements into egg measurements effectively reduces the noise variability of the measurements; however, assuming that the wind is constant over a 25km box may introduce significant errors and disregard valuable information for certain wind/rain fields that exhibit meso-scale structure. As described below, UHR estimation takes a different approach.

The noise-free slice measurement can be written as

$$\sigma^0_{t,s_i} = \iint A_{s_i}(x,y)\sigma^0_{t,s_i}(x,y)dxdy$$
$$= \iint A_{s_i}(x,y)\text{gmf}(\vec{U}(x,y),\theta_{s_i}(x,y),\psi_{s_i}(x,y),p_{s_i})dxdy,$$

where (x,y) is the spatial index, $\sigma^0_{t,s_i}(x,y)$ is the noise-free or 'true' σ^0 field that is sampled by the spatial response function $A_{s_i}(x,y)$ for slice s_i, gmf() is either the wind/rain [3] or wind-only GMF, $\vec{U}(x,y)$ is either the wind/rain or wind-only vector field and, θ_{s_i}, ψ_{s_i}, and p_{s_i} are the incidence angle, the azimuth angle, and the polarization of slice s_i respectively. All of the slice measurements of a given flavor f_j can be stacked into a vector $\vec{\sigma}^0_{t,f_j}$ producing the noise-free measurement model for each flavor

$$\vec{\sigma}^0_{t,f_j} = \begin{bmatrix} \iint A_{s_1}(x,y)\sigma^0_{s_1}(x,y)dxdy \\ \vdots \\ \iint A_{s_{N(f_j)}}(x,y)\sigma^0_{s_{N(f_j)}}(x,y)dxdy \end{bmatrix} \forall f_j,$$

where $N(f_j)$ is the number of measurements of flavor f_j.

For UHR wind retrieval, all the slices of each flavor are assumed to sample the same σ^0 field. That is, $\sigma^0_{s_1}(x,y) = \cdots = \sigma^0_{s_{N(f_j)}}(x,y) = \sigma^0_{f_j}(x,y)$ for each $f_j = 1,2,3,4$. This implies that there is negligible local azimuth and incidence angle variation among slices of the same flavor that cover the same 2.5km pixel. This approximation is appropriate for QuikSCAT because change in the GMF over the main lobe of the slice spatial response functions due to geometry (azimuth and incidence angle) is small. The noise-free measurement model is then

$$\vec{\sigma}^0_{t,f_j} = \begin{bmatrix} \iint A_{s_1}(x,y)\sigma^0_{f_j}(x,y)dxdy \\ \vdots \\ \iint A_{s_{N(f_j)}}(x,y)\sigma^0_{f_j}(x,y)dxdy \end{bmatrix}$$
$$= H_{f_j}(\sigma^0_{f_j}(x,y)) \ \forall f_j,$$

where $H_{f_j}()$ is a linear operator that operates on $\sigma^0_{f_j}(x,y)$–the σ^0 field of flavor f_j. The σ^0 fields of each flavor are assumed to be the result of a wind field projected through the GMF with different geometries for each flavor. That is,

$$\sigma^0_{f_j}(x,y) = gmf(\vec{U}(x,y),\theta_{f_j}(x,y),\psi_{f_j}(x,y),p_{fj}),$$

where $\theta_{f_j}(x,y) = \sum_{s_i} A_{s_i}(x,y)\theta_{s_i}(x,y)/\sum_{s_i} A_{s_i}(x,y)$ is the average incidence angle of the slices of flavor f_j, $\psi(x,y) = \sum_{s_i} A_{s_i}(x,y)\psi_{s_i}(x,y)/\sum_{s_i} A_{s_i}(x,y)$ is the average azimuth angle, and p_{f_j} is the polarization of the slices of flavor f_j.

This formulation allows the slices of the same flavor to be combined to reconstruct four high resolution σ^0 fields (one of each flavor) [8]. The UHR process reconstructs the four σ^0 fields on a 2.5km grid. Then point-wise estimation of both the wind-only and wind/rain vector is performed using only the corresponding pixel from each of the four reconstructed σ^0 fields to yield high resolution wind/rain estimates on a 2.5km grid. Because there is effectively less averaging in the UHR process, the results are typically more noisy than the conventional 25km product; however, meso-scale information is preserved.

III. Reconstruction

This section discusses the reconstruction process. A method [9] of mitigating land contamination is also presented.

A. UHR σ^0 fields

Generation of the four flavors of UHR σ^0 fields is based on incoherent image reconstruction (since the phase is not preserved in the σ^0 measurements). In general we want to reconstruct the spatial σ^0 image for each flavor to the highest resolution possible from the measurements of the slice σ^0's.

In order to obtain $\sigma^0_{f_j}(x,y)$ from each σ^0_{t,s_i} of flavor f_j, the operator $H_{f_j}()$ must be inverted. Since $H_{f_j}()$ operates on a continuous (as opposed to discrete) σ^0 field and there are finitely many slice measurements, $H_{f_j}()$ is not strictly invertible. However, a pseudo-inverse can be found [8]. For the UHR product, a simple approach using the first iteration of the Neumann expansion of the inverse of the operator $H_{f_j}()$ is employed for each flavor separately. The reconstruction operation, commonly known as AVE [10], for flavor f_j can be written as [2]

$$\hat{\sigma}^0_{f_j}(x,y) = \frac{1}{p(x,y)}\sum_{s_i} A_{s_i}(x,y)\sigma^0_{m,s_i}$$

where $p(x,y) = \sum_{s_i} A_{s_i}(x,y)$ is a normalization scale factor, and σ^0_{m,s_i} is the $s_i{}^{th}$ noisy slice measurement for flavor f_j.

In practice, samples of the continuous $\hat{\sigma}^0_{f_j}(x,y)$ fields are reconstructed. Assuming that each $A_{s_i}(x,y)$ is band-limited, the continuous $\hat{\sigma}^0_{f_j}(x,y)$ fields can be exactly represented by regularly spaced samples. The coarsest spacing of the samples from which the continuous signal can be exactly reconstructed (i.e. the resolution) is related to the highest band-limit of the slice response functions. If the slice response functions are assumed to be two-dimensional sinc-squared functions having a narrow (approximately 7km) 6 dB beam-width in one direction and a wide (about 25km) 6 dB beam-width in the other, then the resolution is easily found. A one-dimensional sinc-squared function can be exactly represented by samples spaced at one fourth the width of the main lobe or about half the width of the 6 dB beam-width. For a two-dimensional function, the samples in the direction of the narrow beam-width must be spaced at about half the 6 dB beam-width in order to exactly represent the signal. Thus, the sample spacing must be decreased by a factor of $\sqrt{2}$ to account for the worst case slice orientation (the direction of the narrow beam-width 45^o from the direction of the sample griding). This yields a minimum sample spacing of about $\frac{7}{2\sqrt{2}}$km $\approx$2.5km. Thus, the

samples of $\hat{\sigma}^0_{f_j}(x,y)$ are reconstructed on a regularly spaced 2.5km grid. This results in the implemented reconstruction operation

$$\hat{\sigma}^0_{f_j}[x,y] = \frac{1}{p[x,y]} \sum_{s_i} A_{s_i}[x,y]\sigma^0_{m,s_i},$$

where the square brackets $[x,y]$ represent a discrete index (i.e. samples on the 2.5km grid). While $\hat{\sigma}^0_{f_j}(x,y)$ for each f_j is reconstructed to 2.5km, the effective wind resolution may be lower (estimated to be 6km to 8km).

Note that the reconstruction operation is a function of the exact spatial response function for each slice. For simplicity, the UHR processing code approximates $A_{s_i}(x,y)$ by a function $\tilde{A}_{s_i}(x,y)$ that is constant in the main lobe of the slice spatial response (6 dB) and zero outside the main lobe. This approximation effectively increases the variability of the wind/rain estimates and may also introduce bias errors. Nevertheless these errors are relatively small.

B. Land Contamination Mitigation

When land is present in the σ^0 fields, the relatively high backscatter of land can drown out the wind/rain signal. The land contaminated slice measurements (i.e. slices whose spatial response functions overlap land significantly) may be discarded before the reconstruction. This reduces the impact of land contamination and allows for wind/rain estimates to be within a few km from land (much closer than 30km). This mitigation of land contamination relies on a metric called the land contribution ratio (LCR) defined as [9]

$$LCR \quad = \quad \iint_{R_L} A_{s_i}(x,y)dxdy,$$

where R_L denotes the region of the slice spatial response function that is over land. A simple threshold that is a function of the land σ^0 value and the local wind speed over the ocean is used to discard contaminated slices that lead to poor wind estimates, while preserving those that do not significantly degrade the estimates. The land σ^0 is conservatively estimated by choosing the largest slice σ^0 whose center is over land in the region near the slice of interest. The local wind speed is conservatively estimated as the lowest wind speed of the 25km QuikSCAT product near the slice of interest. The threshold is then calculated and the slice is discarded if the LCR is greater than the threshold [9].

Fig. 1 shows the 6dB slice contours for one flavor overlapping the reconstructed σ^0 field after discarding land contaminated slices. Information that would be discarded in the 25km product (such as the region between the channel islands and the California mainland) is preserved without introducing land contamination. Note that because fewer measurements may be used to estimate the winds in the near coastal zone due to LCR-based removal, the near coastal estimates tend to be noisier than those not near land. Improving wind direction and rain retrieval in such cases are topics of ongoing investigation.

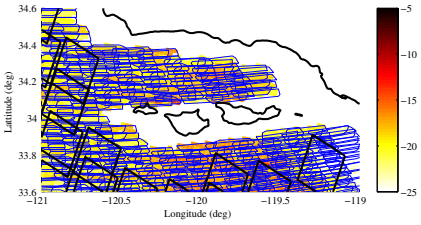

Fig. 1. Land contamination case near the channel islands off the coast of California. The 6dB slice contours for one σ^0 flavor (h-pol fore-looking) are superimposed on the reconstructed σ^0 field in dB after discarding land contaminated slices. The large black squares represent the locations of the conventional 25km wind product wind vector cells.

IV. UHR Wind/Rain Estimation

This section presents the theory and assumptions made in point-wise UHR wind-only and simultaneous wind/rain retrieval. Maximum likelihood (ML) estimation, ambiguity selection, and maximum aposteriori (MAP) estimation are all outlined and a derivation of the likelihood function is presented.

A. Derivation of Likelihood Function

UHR wind/rain estimation relies on the probability density function (or likelihood function) of the four flavors of point-wise σ^0 measurements ($\vec{\sigma}^0[x,y]$) given the 'true' (or noise free) vector of point-wise σ^0 measurements ($\vec{\sigma}^0_t[x,y]$) for every pixel at discrete spatial index $[x,y]$ on the 2.5km grid. This density function is defined as $f(\vec{\sigma}^0[x,y]|\vec{\sigma}^0_t[x,y])$. Here this function is derived from the standard noise model of the slice measurements.

Recall the standard assumption that each slice measurement is an independent Gaussian random variable with mean σ^0_{t,s_i} and variance $(K_{p,s_i}\sigma^0_{t,s_i})^2$. Since the reconstruction operation is linear, it can be shown that the reconstructed σ^0 at each pixel is also a Gaussian random variable where each flavor is independent. The mean of each pixel $[x,y]$ of the σ^0 field of flavor f_j is

$$E\{\hat{\sigma}^0_{f_j}[x,y]\} \quad = \quad \sum_{s_i} \tilde{A}_{s_i}[x,y]\sigma^0_{t,s_i} \equiv \quad \mu_{f_j}[x,y],$$

and the covariance of pixel $[x,y]$ and pixel $[z,\tau]$ is

$$\mathrm{cov}(\hat{\sigma}^0_{f_j}[x,y], \hat{\sigma}^0_{f_j}[z,\tau]) = \sum_{s_i} \tilde{A}_{s_i}[x,y]\tilde{A}_{s_i}[z,\tau]K^2_{p,s_i}(\sigma^0_{t,s_i})^2.$$

Note that after reconstruction each pixel is correlated with several other pixels of the same flavor. Nevertheless, point-wise estimation assumes that each pixel is independent. We assume that the variance can be written as

$$(\xi_{f_j}[x,y])^2 = \sum_{s_i} \tilde{A}^2_{s_i}[x,y]K^2_{p,s_i}(\mu_{f_j}[x,y])^2 = (\mu_{f_j}[x,y])^2K^2_p,$$

where $K^2_p \equiv \sum_{s_i} \tilde{A}^2_{s_i}[x,y]K^2_{p,s_i}$ [2] and $\xi_{f_j}[x,y]$ is the standard deviation. This assumption may increase the variability of the estimates since the spatial correlation (which we are neglecting) acts like a low-pass filter producing spatially

smoothed estimates. The desired likelihood function for a given pixel $[x, y]$ becomes

$$f(\vec{\sigma}^0[x,y]|\vec{\sigma}_t^0[x,y]) = \prod_{f_j} f(\hat{\sigma}_{f_j}^0[x,y]|\mu_{f_j}[x,y])$$
$$= \prod_{f_j} \frac{1}{\sqrt{2\pi}\xi_{f_j}[x,y]} \exp\left\{\frac{-(\hat{\sigma}_{f_j}^0[x,y] - \mu_{f_j}[x,y])^2}{2(\xi_{f_j}[x,y])^2}\right\}$$
$$= f(\vec{\sigma}^0[x,y]|\vec{\mu}[x,y]),$$

where $\vec{\mu}[x, y])$ is the vector of the means of the four flavors of σ^0 at index $[x, y]$.

B. ML Estimation

Given the point-wise likelihood function, we can estimate the wind or simultaneously estimate the wind/rain vector [3] at every pixel via ML estimation. In the ideal case, ML estimation uses the probability density function of the σ^0 slice measurements given the wind (and/or rain), i.e. $f(\vec{\sigma}^0[x,y]|\vec{U}[x,y])$. However, because of the non-linearity of the GMF it is difficult to obtain $f(\vec{\sigma}^0[x,y]|\vec{U}[x,y])$ from the noise model. Nevertheless, all of the information about the wind/rain that is known from the measurements is contained in another density function $f(\vec{\sigma}^0[x,y]|\vec{\sigma}_t^0[x,y])$ or equivalently $f(\vec{\sigma}^0[x,y]|\vec{\mu}[x,y])$. For convenience we use $f(\vec{\sigma}^0[x,y]|\vec{\mu}[x,y])$ in place of $f(\vec{\sigma}^0[x,y]|\vec{U}[x,y])$. This is appropriate since knowing $\vec{\mu}[x,y]$ provides no more information about $\vec{\sigma}^0[x,y]$ than knowing $\vec{U}[x,y]$. Nevertheless, there are subtle consequences of this assumption that manifest themselves in the form of statistical biases in the estimates. That is, certain wind/rain vectors are less likely to be estimated than other wind/rain vectors. Using $f(\vec{\sigma}^0[x,y]|\vec{\sigma}_t^0[x,y])$ rather than $f(\vec{\sigma}^0[x,y]|\vec{U}[x,y])$ is equivalent to estimating $\vec{\sigma}_t^0[x,y]$ from measurements of $\vec{\sigma}^0[x,y]$ in the subspace of σ^0 measurements that get mapped to from the wind/rain space through the GMF and then providing all the wind/rain vectors that produce the estimate of $\vec{\sigma}_t^0[x,y]$ as ambiguous wind/rain estimates.

The resulting maximum likelihood estimate of the wind/rain vector for pixel $[x, y]$ ($\hat{\vec{U}}_{ML}[x,y]$) is

$$\hat{\vec{U}}_{ML}[x,y] = \underset{\vec{U}[x,y]}{\text{argmax}}\{f(\vec{\sigma}^0[x,y]|\vec{\sigma}_t^0[x,y])\} \quad (1)$$
$$= \underset{\vec{U}[x,y]}{\text{argmin}} \left\{\sum_{f_j} \frac{(\hat{\sigma}_{f_j}^0 - \mu_{f_j}[x,y])^2}{2(\xi_{f_j}[x,y])^2} + \log(\xi_{f_j}[x,y])\right\},$$

where $\vec{U}[x, y]$ is any wind/rain vector at pixel $[x, y]$, and $\mu_{f_j}[x, y]$ and $\xi_{f_j}[x, y]$ are functions of $\vec{U}[x, y]$. The same formulation for the ML estimator applies to wind-only and simultaneous wind/rain estimation. For wind-only retrieval the vector $\vec{U}[x, y]$ includes each vector component of the wind (either speed and direction or u and v) at pixel $[x, y]$. For simultaneous wind/rain retrieval $\vec{U}[x, y]$ includes the wind vector components as well as the rain rate at pixel $[x, y]$. Typically, there are multiple $\vec{U}[x, y]$ that maximize (1) resulting in wind-only and wind/rain estimate ambiguities for each pixel. For UHR processing, the four highest wind/rain ambiguities and the four highest wind-only ambiguities are found and ranked according to likelihood value (the wind-only and wind/rain ambiguities are stored separately producing two vectors of ambiguities for each pixel).

C. Ambiguity Selection

In order to obtain a unique estimate of the wind or wind/rain field, an ambiguity selection algorithm must be performed after ML estimation of the wind/rain. Because of noise, the skill (percentage of first ambiguities or highest ranked ambiguities that are closest to the 'true' wind/rain vector) for the UHR product is relatively poor compared to the 25km product. In both cases outside data is used to select the best ambiguities. In the current UHR wind-only and wind/rain ambiguity selection algorithms, the ambiguity whose wind vector components are closest to the 25km QuikSCAT product is chosen (a procedure called nudging) and then median filtering is performed. Alternatively, model-based or field-wise estimates may be used to nudge ambiguity selection; however, these are not yet implemented in the current UHR product.

D. MAP Estimation

The UHR product also provides an alternate wind retrieval approach that is based on MAP estimation. MAP estimation is similar to ML estimation, only the likelihood function is scaled by a prior probability density function of the wind/rain $f(\vec{U}[x,y])$. The MAP estimate can be written as

$$\hat{\vec{U}}_{MAP}[x,y] = \underset{\vec{U}[x,y]}{\text{argmax}}\{f(\vec{\sigma}^0[x,y]|\vec{\sigma}_t^0[x,y])f(\vec{U}[x,y])\},$$

where $f(\vec{U}[x,y])$ is a prior based on either a field-wise model fit to the data, outside data, or a climatological model of wind/rain phenomena. [4] and [5] develop a field-wise hurricane model for wind/rain fields which provides point-wise prior distributions whose parameters are estimated from the scatterometer data. The UHR product provides this option for measurements over tropical cyclones. Furthermore, outside data such as numerical weather predictions, for example the product provided by the National Centers for Environmental Prediction (NCEP), can be used to provide a prior.

The UHR product includes an option to report MAP estimates using a Gaussian prior for the wind where the mean is the NCEP wind prediction spatially interpolated to the 2.5km grid spacing and the variance is constant. This allows for MAP estimates for wind structures beyond just hurricanes.

V. Data Description and Examples

This section overviews the trade-offs between the different UHR products. A description of the UHR data files is provided. Examples are presented and the strengths and limitations of each product are described.

Each UHR file contains several data sets: the ML estimation-derived wind-only and wind/rain ambiguities, the MAP estimation wind and wind/rain ambiguities from an NCEP prior, the MAP estimation wind and wind/rain ambiguities for the hurricane model based prior (where appropriate),

TABLE I

HDF SDS ARRAYS WITHIN THE BYU L2H FILES. THESE DATA SETS ARE IN EVERY L2H FILE.

Data set name	Description
ascnode	indicates whether the data is from an ascending or descending pass
swath_indicies	vector of along-track and cross-track starting and ending indicies on ultra high resolution grid
latitude	latitude index of each pixel
longitude	longitude index of each pixel
land_mask	flags land or water for each pixel
wind_speed	wind-only wind speed ambiguities (m/s) in ML value order
wind_dir	wind-only wind direction ambiguities (deg) in ML value order
max_likelihood_est	ML value from wind retrieval
num_ambigs	number of wind-only ambiguities at each pixel
wvc_selection	index (1 to 4) of selected wind-only ambiguity
wvc_selection2	index of alternate ambiguity selection
wind_speed_L2B	L2B wind speeds (m/s) interpolated to 2.5km
wind_dir_L2B	L2B wind directions (deg) interpolated to 2.5km
wind_speed_ncep	NCEP wind speeds (m/s) interpolated to 2.5km
wind_dir_ncep	NCEP wind directions (deg) interpolated to 2.5km
wvc_quality_flag	copy of L2B wvc_quality_flag on 2.5km grid

TABLE II

HDF SDS ARRAYS IN THE BYU L2H FILES WHEN SIMULTANEOUS WIND/RAIN (SWR) ESTIMATION IS PERFORMED. THIS DATA IS INCLUDED ONLY IN SELECTED L2H FILES.

Data set name	Description
wind_speed_swr	SWR wind speed ambiguities (m/s) in ML value order
wind_dir_swr	SWR wind direction ambiguities (deg) in ML value order
rain_rate_integrated	SWR rain rate ambiguities (km mm/hr) in ML value order (calibrated to TRMM-PR)
rain_rate_surface	alternate rain rate ambiguities (mm/hr) in ML value order (calibrated to AMSR)
max_likelihood_est_swr	ML value from wind/rain retrieval
num_ambigs_swr	number of ambiguities at each pixel
wvc_selection_swr	index (1 to 4) of selected SWR ambiguity from median-filter-based ambiguity removal
percent_rain	inferred rain fraction for each ambiguity
regime	estimated wind/rain retrieval regime. 0 = rain does not significantly affect wind 1 = rain and wind backscatter are of same order 2 = rain dominates wind
wvc_selection_opt	ambiguity selection index (1 to 4) from combined SWR and wind-only retrieval
set_selection_opt	flag to indicate which retrieval method is used for each pixel. Used with wvc_selection_opt. 0 = value of wvc_selection_opt is from SWR 1 = value of wvc_selection_opt is from wind-only retrieval
rain_confidence_flag	rain estimate quality confidence flag 0 = Low confidence in estimated rain 1 = High confidence in estimated rain

the field-wise hurricane model fit wind and rain fields (where appropriate), and the selected ambiguities for each wind or wind/rain data set. All of these data sets are stored in hierarchal data format (HDF) in the same file called the BYU L2H file. This ensures that each data set is co-registered and is convenient for the end user. The reconstructed σ^0 field images (with or without LCR processing) are currently stored in a separate file in binary format called the 'avewr' file. Tables I, II, and III name and briefly describe the possible scientific data sets (SDS) in the L2H wind/rain files. The data sets in Table I are in every L2H file, but the data in Tables II and III are only included if simultaneous wind/rain retrieval and/or MAP estimation are performed.

The UHR product provides high resolution (2.5km pixel spacing) wind, rain, and reconstructed σ^0 fields for localized regions of interest. The UHR product is appropriate for studying wind and rain phenomena on a scale of 500km or less. The product may be too noisy to be useful in global scale studies. For such studies, the standard 25km products are more appropriate. Using wind-only products is appropriate when studying cases where rain rates are not significant or in coastal regions. The wind/rain products are more appropriate wherever rain rates are significant. The MAP estimates can be considered when meso-scale detail is desired, but less noise than the ML result is also desired.

Fig. 2 shows an example of rain estimates in a hurricane (Isaac Sept 29, 2000). The ML wind/rain rain rates, the MAP wind/rain rain rates, and the corresponding rain rate measurements from the Tropical Rainfall Measuring Mission Precipitation Radar (TRMM-PR) are shown. A plot of the mean of the ML and MAP rain rates as a function of the TRMM-PR rain rate is also provided. The MAP rain estimates are more consistent with the TRMM-PR data and there are much fewer rain false alarms than the ML-based rain estimates. Fig. 3 shows the corresponding ML and MAP wind field estimates, along with the conventional 25km wind field for the same storm observation as in Fig 2. The 25km wind product does not resolve the eye and fine scale structures well and the direction estimates exhibit some cross-track bias typical of rain contamination. The UHR MAP wind speed and direction estimates are less biased, less noisy, and exhibit less artifacts of the heavy rain band in the upper left quadrant of the storm compared to the UHR ML wind estimates; however, relatively fine detail compared to the 25km product is preserved.

VI. CONCLUSION

The UHR QuikSCAT product has advantages and limitations. The theory and assumptions involved in the UHR product and the conventional 25km product are contrasted, and trade-offs and suggested usage are discussed. A data description of the UHR product is provided and some examples are presented. The UHR product provides wind and rain data at a high enough resolution to study many interesting meso-scale phenomena, although the estimates are noisier than the standard 25km product. Furthermore, UHR makes possible an effective near coastal QuikSCAT product.

REFERENCES

[1] D. G. Long, "High resolution wind retrieval from SeaWinds," *IGARSS*, pp. 751–753, 2002.

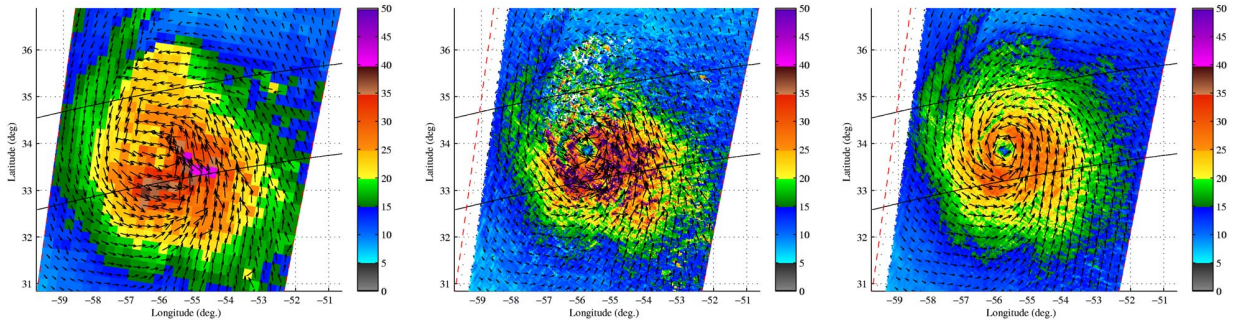

Fig. 3. Wind speed fields (m/s) with superimposed vectors in Hurricane Isaac Sept 29, 2000 derived from (left) the standard 25km processing, (center) UHR ML-based wind/rain estimation, and (right) MAP-based wind/rain estimation. The UHR vectors are down-sampled by 10 for plotting.

TABLE III

HDF SDS ARRAYS CONTAINED IN THE BYU L2H FILES DERIVED FORM HURRICANE MODEL-BASED MAP WIND-ONLY (HMMAP), HURRICANE MODEL-BASED MAP SIMULTANEOUS WIND/RAIN ESTIMATION (HMMAPSWR), AND NCEP BASED MAP ESTIMATION (NCEPMAP). THESE DATA SETS ARE INCLUDED ONLY IN SELECTED L2H FILES.

Data set name	**Description**
hurricane_model_params	hurricane model parameters
wvc_selection_map	index (1 to 4) of selected point-wise UHR (wind-only) ambiguity based on MAP ambiguity selection
map_model_speed	hurricane model fit speed field
map_model_dir	hurricane model fit direction field
map_model_rain	hurricane model fit rain field
wind_speed_map	HMMAP estimation wind speed ambiguities (m/s) in MAP value order
wind_dir_map	HMMAP estimation wind direction ambiguities (deg) in MAP value order
wind_speed_map_swr	HMMAPSWR estimation wind speed ambiguities (m/s) in MAP value order
wind_dir_map_swr	HMMAPSWR estimation wind direction ambiguities (deg) in MAP value order
rain_rate_map_swr	HMMAPSWR estimation integrated rain rate ambiguities (m/s) in MAP value order
max_aposteriori_prob_est	HMMAP value from MAP wind retrieval
num_ambigs_map	number of HMMAP ambiguities at each pixel
max_aposteriori _prob_est_swr	HMMAPSWR value from MAP wind/rain retrieval
num_ambigs_map_swr	number of HMMAPSWR ambiguities at each pixel
wvc_selection_ncep	index (1 to 4) of selected UHR (wind-only) ambiguity using NCEP based MAP ambiguity selection
wind_speed_ncep	NCEPMAP estimation wind speed ambiguities (m/s) in MAP value order
wind_dir_ncep	NCEPMAP estimation wind direction ambiguities (deg) in MAP value order
max_aposteriori _prob_est_ncep	NCEPMAP value from MAP wind retrieval
num_ambigs_map_ncep	number of NCEP based MAP ambiguities at each pixel

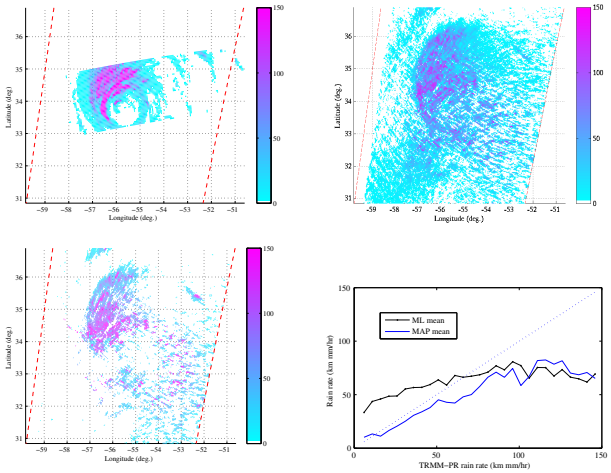

Fig. 2. Rain estimates in Hurricane Isaac Sept 29, 2000 derived from (upper left) TRMM-PR, (upper right) UHR ML-based wind/rain estimation, (lower left) MAP-based wind/rain estimation, and (lower right) plot of bias of ML- and MAP-based estimates as a function of TRMM-PR rain rate.

[2] D. G. Long, J. B. Luke, and W. Plant, "Ultra high resolution wind retrieval from SeaWinds," *IGARSS*, pp. 1264–1266, 2003.

[3] M. P. Owen and D. G. Long, "Progress toward validation of QuikSCAT ulrta-high-resolution rain rates using TRMM PR," *IGARSS*, 2008.

[4] B. A. Williams and D. G. Long, "Estimation of hurricane winds from SeaWinds at ultra high resolution," *IEEE Transactions on Geoscience and Remote Sensing*, 2008.

[5] ——, "Rain and wind estimation from SeaWinds in hurricanes at ultra high resolution," *IGARSS*, 2008.

[6] T. Lungu, *QuikSCAT Science Data Product Users Manual Overview and Geophysical Data Products*, September 2006.

[7] D. W. Draper and D. G. Long, "Evaluating the effect of rain on seawinds scatterometer measurements," *Journal of Geophysical Research*, vol. 109, no. C02005, 2004.

[8] D. S. Early and D. G. Long, "Image reconstruction and enhanced resolution imaging from irregular samples," *IEEE Transactions on Geoscience and Remote Sensing*, vol. 39, no. 2, pp. 291–302, 2001.

[9] M. P. Owen and D. G. Long, "Land contamination compensation for QuikSCAT near-coastal wind retrieval," *IEEE Transactions on Geoscience and Remote Sensing*, vol. 47, pp. 839–850, 2009.

[10] D. G. Long, P. J. Hardin, and P. T. Whiting, "Resolution enhancement of spaceborne scatterometer data," *IEEE Transactions on Geoscience and Remote Sensing*, vol. 31, 1993.